Journal of Biomaterials Science, Polymer Edition

ISSN: 0920-5063 (Print) 1568-5624 (Online) Journal homepage: http://www.tandfonline.com/loi/tbsp20

In Vitro Cell Uptake of Biocompatible Magnetite/Chitosan Nanoparticles with High Magnetization: A Single-Step Synthesis Approach for In-Situ-Modified Magnetite by Amino Groups of Chitosan

Yongliang Wang , Baoqiang Li , Feng Xu , Dechang Jia , Yujie Feng & Yu Zhou

To cite this article: Yongliang Wang , Baoqiang Li , Feng Xu , Dechang Jia , Yujie Feng & Yu Zhou (2012) In Vitro Cell Uptake of Biocompatible Magnetite/Chitosan Nanoparticles with High Magnetization: A Single-Step Synthesis Approach for In-Situ-Modified Magnetite by Amino Groups of Chitosan, Journal of Biomaterials Science, Polymer Edition, 23:7, 843-860, DOI: 10.1163/092050611X562166

To link to this article: http://dx.doi.org/10.1163/092050611X562166

Published online: 13 Apr 2012.

VSP

Journal of Biomaterials Science 23 (2012) 843–860

Journal of BIOMATERIALS SCIENCE
brill.nl/jbs

In Vitro Cell Uptake of Biocompatible Magnetite/Chitosan Nanoparticles with High Magnetization: A Single-Step Synthesis Approach for *In-Situ*-Modified Magnetite by Amino Groups of Chitosan

Yongliang Wang [a], **Baoqiang Li** [a,b,*], **Feng Xu** [b], **Dechang Jia** [a], **Yujie Feng** [a] **and Yu Zhou** [a]

[a] Institute for Advanced Ceramics and State Key Laboratory of Urban Water Resource and Environment, Harbin Institute of Technology, P. O. Box 433, Harbin 150001, P. R. China
[b] HST-Center for Biomedical Engineering, Department of Medicine Brigham and Women's Hospital, Harvard Medical School, Boston, MA 02139, USA

Received 30 November 2010; accepted 14 February 2011

Abstract

Current attempts for synthesizing chitosan-modified magnetite nanoparticles (CS-MNPs) as drug carrier involve use of surfactants, which brings potential cytotoxicity and decrease of saturated magnetization (Ms). To address this, we developed a facile single-step method for synthesizing CS-MNPs. The developed method offers several advantages. No surfactant was involved and the magnetite nanoparticles were *in-situ*-coated with a chitosan (CS) layer, which endows the CS-MNPs with enhanced physical and chemical properties. The Ms of magnetite was significantly increased (55.5 emu/g) as compared to magnetite nanoparticles modified by surfactants with oxygen ligands, indicating their potential applications as drug-delivery systems (DDSs) where high saturated magnetization (Ms) is preferred. Besides, the amount of CS layer of CS-MNPs was approx. 24 wt%, which makes the synthesized CS-MNPs highly biocompatible as no acute adverse effect of the viability on MG-63 cells was observed at doses up to 0.2 mg/ml. Macropinocytosis is the main endocytic mechanism of MG-63 cells internalize CS-MNPs, which might avoid lysosomal degradation of the CS-MNPs. The synthesized CS-MNPs have potential applications in the fields of targeted drug delivery, separation for purification and immunoassay and magnetic resonance imaging.

Keywords

Chitosan, magnetite, amino groups, saturated magnetization, intracellular uptake

1. Introduction

Cancer is a group of diseases characterized by uncontrolled growth of abnormal cells. It is estimated that there are more than 12 million new cancer cases

* To whom correspondence should be addressed. E-mail: libq@hit.edu.cn

 DOI:10.1163/092050611X562166

worldwide annually, and the total number of deaths by cancer was 7.6 million in 2007 alone [1]. With the improvements of cancer chemotherapy, the survival rates have increased significantly (5-year relative survival from approx. 45% in 1994 to approx. 65% in 2002) [2]. However, chemotherapy can induce significant side-effects (e.g., acute interstitial pneumonitis, radiation recall dermatitis) weakening the treating quality [3]. Different targeted drug-delivery systems (DDSs), such as polymeric nanoparticles, liposomes, micelles and magnetic nanoparticles, have been developed to minimize or avoid the side-effects through delivering drugs to specific cells/tissues [4–8]. Among these systems, magnetic nanoparticles (e.g., Fe_3O_4-(dextran-g-poly(NIPAAm-*co*-DMAAm), Fe_3O_4-YCC-DOX, Fe_3O_4-(glycerol monooleate)) are advantageous due to the combination of the intrinsic properties of the magnetic nano-core with their drug-loading capability that can be bestowed on a suitable layer [9–11].

The magnetic nano-core endows the magnetic nanoparticles (MNPs) with target properties through an external magnetic field. However, there is a main limitation of magnetic nanoparticles for DDS. The magnetic nano-core must be superparamagnetic to avoid agglomeration once the external magnetic field is removed, limiting the diameter of magnetic nano-core to less than 30 nm. This size limitation of magnetic nano-cores implies a reduced magnetic response. Thus, magnetic nano-cores with high saturated magnetization (Ms) are preferred for remote controlling the distribution and the location of DDS *in vivo* facilely through modulating the direction and strength of harmless magnetic field.

It has been proven that the ligands of coating layers have a remarkable influence on the physical properties (especially Ms) of MNPs. Cordente *et al.* have proved that a coating layer with donor ligands (such as amines) does not reduce the magnetization of the nickel nanoparticles, whereas the use of trioctylphosphine oxide leads to the reduction in the magnetization [12]. Deng *et al.* synthesized silica-coated MNPs and they found that a significant decrease of Ms (from 48 to 30 emu/g, approximately) was expressed after silica coating [13]. It is thought that the Fe–O–Si connection decreased the Ms of silica-coated MNPs. Unfortunately, the existing coating layers (e.g., silica dioxide, poly(ethylene glycol), polythiophene) usually have ligands with O atom (e.g., CO, COOH, OH), which induced a significant decrease of Ms [13–16], giving rise to the problem that a stronger external magnetic field, which might hurt the body, has to be applied in order to locate the magnetic nanoparticles accurately and non-invasively. Chitosan (CS), with free primary amino groups which have little effect on Ms [17], has the potential to address the problem of the decreased Ms. Other attractive characteristics of chitosan include: (i) non-toxicity, biocompatibility and biodegradability; (ii) reactive groups ($–NH_2$ and –OH) which can link extensive kinds of targeted drugs; (iii) high solubility at pH 5.3 (the pH of abnormal cells) and insolubility at pH 7.4 (the physiological condition), which makes it easy to release the targeted drug in the abnormal cells due to the pH sensitivity of CS [18]. These characteristics, along with its broad and easy acquisition from nature, make CS suitable as coating layer for MNPs.

The conventional method for fabrication of chitosan modified magnetite (CS-MNPs) consists of two main steps, i.e., synthesis of MNPs and encapsulation of these MNPs in CS [18–21]. However, there are several challenges associated with the conventional method. Firstly, during MNPs synthesis, surfactants are required to avoid the aggregation of MNPs. Unfortunately, the surfactants usually have ligands with O atom (e.g., Span-80, D-monnos, lactobionic acid, sodium oleate, poly(ethylene glycol)) [22], which induced decreased Ms. Secondary, the surfactants might induce potential cytotoxicity [23]. Finally, during MNPs encapsulation, the oxidation of MNPs was inevitable, which also induced a decrease of Ms.

To address the above challenges with current CS-MNPs methods, in this study we developed a facile single-step way for synthesizing CS-MNPs using an in-situ modified magnetite by amino groups of chitosan, which brings a high Ms of CS-MNPs. The method can solve the challenges as mentioned above. Firstly, no surfactant was involved, which avoided the influence of surfactant. Secondly, the oxidation during encapsulation of MNPs was avoided. Moreover, the internalization mechanism of CS-MNPS into MG-63 cells was discussed.

2. Materials and Methods

2.1. Materials

Biomedical-grade CS (viscosity-average molecular weight 3.4×10^5) with 91.4% deacetylation was supplied by Qingdao Haihui Bioengineering. Ferric chloride hexahydrate ($FeCl_3 \cdot 6H_2O$) and ferrous chloride tetrahydrate ($FeCl_2 \cdot 4H_2O$) were acquired from Tianjin Kemiou. 3-(4,5-dimethyl-thiazol-2yl)-2,5-diphenyl tetrazolium bromide was obtained from Sigma. All chemicals were analytic grade reagents and used without further purification.

2.2. Synthesis of CS-MNPs

The CS-MNPs was synthesized as follows. Briefly, chitosan solution (4%, g/g) was cast on the internal surface of mold and the mold was soaked in NaOH solution (1.25 M) for 2 h to precipitate a CS membrane. CS (4 g) was first dissolved in 100 ml acetic acid solution (2%, v/v). Of a 1 M HCl solution 25 ml was added into the CS solution. The mixture was vigorously stirred for 2 h. Secondly, 8 ml magnetite precursor containing 7 mmol Fe(III) and 3.5 mmol Fe(II) was added into the CS solution. The mixture was loaded into a prepared CS membrane and soaked in NaOH solution (1.25 M) for 6 h, forming a CS-MNPs hydrogel. In order to obtain CS-MNPs, the synthesized CS-MNPs hydrogel was dissolved in 200 ml acetic acid solution (2%, v/v). CS-MNPs were obtained by centrifugation at $12\,000 \times g$ for 10 min.

2.3. Characterization of CS-MNPs

The crystal structure of the CS-MNPs was investigated by X-ray diffraction (Rigaku D/max-2550) using Cu Kα radiation. Transmission Electron Microscopy (FEI Tecnai F20 G2) was used to obtain the morphology of the CS-MNPs. The magnetic

properties were determined by a Physical Property Measurement System (PPMS-9, Quantum Design). The CS content of CS-MNPs was determined by thermal gravity and differential thermal analysis (TG-DTA) (STA 449C, Netzsch). X-ray photoelectron spectroscopy (XPS, K-Alpha, Thermo Fisher) was used to indentify the sorption sites and the interactions between MNPs and CS. The surface charge and hydrodynamic (HD) size of the CS-MNPs were measured by laser scattering (BI-90Plus, Brookhaven) at pH 5.0 in order to avoid the aggregation of CS-MNPs.

2.4. MG-63 Cell Testing

2.4.1. Cytotoxicity

The human osteosarcoma cells (MG-63) cells were cultured in 96-well tissue-culture plates (Corning) at a density of 4×10^4 cells/well and incubated for 24 h. Then the cell medium was replaced with 100 μl medium containing CS-MNPs (three different concentrations: 0.05, 0.10, 0.2 mg/ml) and incubated for 48 h. The cytotoxicity was evaluated by determining the viability of MG-63 at 24 and 48 h, using the MTT test. Cells cultured in cell medium only served as control.

2.4.2. Morphology of CS-MNPs in MG-63 Cells

For morphology characterization, the cells were fixed in 2.5% glutaraldehyde for 2 h and washed with 0.1 M PBS for 3×10 min. Then the cells were fixed in osmium tetroxide for 2 h and washed again with 0.1 M PBS for 3×10 min. After that, the samples were dehydrated in ascending concentrations of ethanol (50, 70, 80, 90, 95 and 100%, 15 min each) and embedded in Spurr resin. Finally, transmission electron microscopy (H-7650, Hitachi) was used to observe the morphology of the CS-MNPs in MG-63 after the samples were cut ultra-thin. ImageJ (National Institutes of Health) was used to analyze the TEM micrographs to obtain the intracellular amount of CS-MNPs (details are given in the Appendix).

3. Results and Discussion

3.1. Synthesis of CS-MNPs

Different from the common two-step method, a facile single-step method was developed for synthesizing CS-MNPs. Fe(II) and Fe(III) were chelated with the active groups of CS (–NH_2 and –OH) and a CS–Fe(II,III) complex was formed. When the CS–Fe(II,III) complex encountered OH^-, the chelated Fe(II) and Fe(III) provided a nucleation site for MNPs. The MNPs were coated *in situ* with CS during nucleation and crystal growth. Due to the chelation effect between –NH_2 groups and Fe(II,III), a weak interaction formed between CS (*via* –NH_2 and –OH groups) and magnetite was synthesized.

3.2. Physical and Magnetic Properties of CS-MNPs

X-ray diffractometry and Raman spectroscopy were used to characterize the crystal structure of CS-MNPs, and the results indicated that the magnetic nanoparticles were magnetite, rather than γ-Fe_2O_3 (see the Appendix).

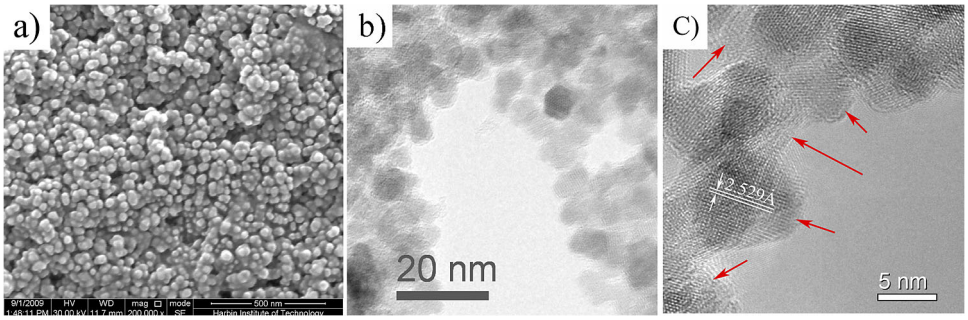

Figure 1. The morphology of synthesized CS-MNPs. (a) SEM morphology (scale bar = 500 nm); (b and c) HRTEM images of CS-MNPs. This figure is published in colour in the online edition of this journal, which can be accessed *via* http://www.brill.nl/jbs

The morphology of CS-MNPs synthesized *via* a single-step reaction is shown in Fig. 1. A slight aggregation (agglomerates of about 35 nm in diameter were observed in Fig. 1a) was due to the CS layer on the magnetite nanoparticles. The hydrogen bond interactions among several CS chains resulted in the entanglement and aggregation of CS-MNPs. Similar observations have been reported earlier. The MNPs, when coated with proteins and polysaccharides (such as dextran), have a tendency to form clusters [25]. Moreover, the specimen preparation process might to some extent bring aggregation of the CS-MNPs. Further insight into the CS-MNPs was given by HRTEM images (Fig. 1b and c). The lattice fringe of $d =$ 2.529 Å agrees well with the (311) lattice plane of magnetite. Moreover, it can be seen that there is a blurry layer which surrounds the magnetite nanoparticles (approx. 10 nm in diameter, red arrows in Fig. 1c). Combined with the XRD pattern, the layer on magnetite was confirmed to be CS.

The values of Ms of MNPs have been reported to be in the range of 30–50 emu/g (see Table 1 for details). Figure 2 shows the hysteresis loop of CS-MNPs in this report at 300 K, and the Ms was 55.5 emu/g. It can be concluded from Table 1 that, compared with the coating layer with O ligands, chitosan with amino groups is preferred for MNPs with high Ms. The might reason is that amino groups lead to less quenching of the surface magnetic moments than ligands with O atom [15], which in turn resulting in CS-MNPs with higher magnetization than reported in the literature. Moreover, the facile single-step synthesis is somewhat beneficial for CS-MNPs with higher Ms.

3.3. CS Layer of CS-MNPs

FT-IR was used to characterize the surface state of CS-MNPs, which indicated the existence of the CS layer of CS-MNPs and the CS layer endowed CS-MNPs with positive charge at physiological pH (7.4) (see the Appendix). TG was used to confirm the amount of CS layer of synthesized CS-MNPs. As can be seen in Fig. 3, in the range of 200–800°C, the CS-MNPs experienced a 24% weight loss which was

Table 1.
The Ms of magnetite nanoparticles synthesized from different conditions

Coating layer	Ligand	Particle size (nm)	Ms (emu/g)
Sodium oleate [16]	–COOH	8	41
Poly(ethylene glycol) [17]	–OH	10	31.3
Span-80 [22]	–OH	20	37.3
None [24]		9	40
Chitosan	$–NH_2$	10	55.5

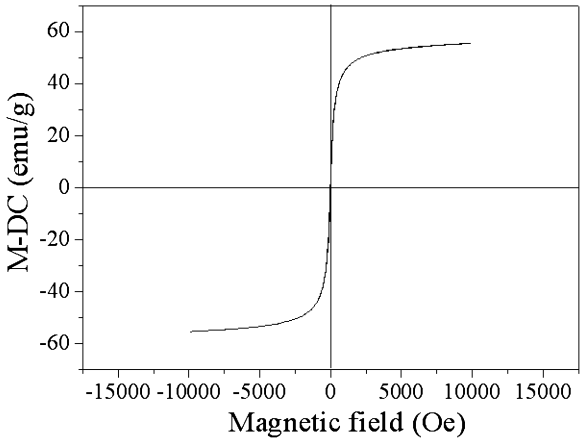

Figure 2. The hysteresis loop of MNPs at 300 K. 17 mg sample was used.

attributed to the decomposition of CS. Considering the 91.4% degree of deacetylation, there were 1.4 mmol/g amino groups and 3 mmol/g hydroxyl groups of the synthesized CS-MNPs, which provide reactive groups for functionalization.

To indentify the sorption sites and the interactions between MNPs and CS, the N_{1s} XPS spectra were determined (Fig. 4). The binding energy (BE) at 397.7 eV was attributed to 'free' amino groups ($–NH_2$) of CS, and the BE at 399.5 eV was assigned to the amino groups which were involved in hydrogen bonds ($–NH_2$–O). However, the BE of 'free' amino groups (397.7 eV) disappeared for CS-MNPs when compared with CS, which might be due to a weak interaction between amino groups and magnetite ($–NH_2$–Fe). This weak interaction between amino groups and magnetite ($–NH_2$–Fe), similar to hydrogen bonds, is environment-sensitive. The O_{1s} XPS spectra of CS and CS-MNPs are also shown in Fig. 5. As can be seen from Fig. 5a and b, similar observations were made for O_{1s} BEs. However, the atomic fractions (AFs) were evidently different. As can be seen from Fig. 5a, the AF at 531.4 eV ('free' hydroxyl groups (–OH)) and the AF at 533.4 eV (C–O–C of chitosan, hydroxyl groups involved in hydrogen bonds (–OH–O and –OH–N)) were 70.2 and 29.8%, respectively. However, for CS-MNPs, AF at 530.1 eV (Fe–O

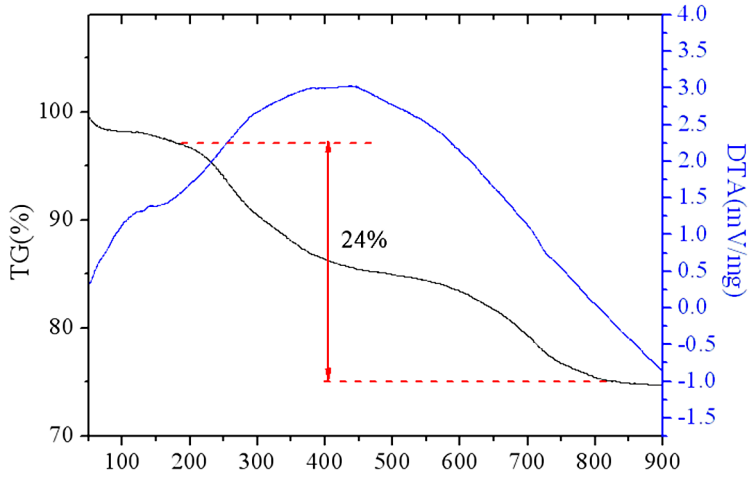

Figure 3. TG-DTA curve of CS-MNPs (approx. 20 mg of each sample, under air atmosphere, gas flow 5 ml/min, heating velocity 10°C/min). This figure is published in colour in the online edition of this journal, which can be accessed *via* http://www.brill.nl/jbs

of MNPs), 531.5 eV (–OH) and 533.0 eV (C–O–C, –OH–O, –OH–N and –OH–Fe) were 17, 21.7 and 61.3%, respectively (Fig. 5b). Compared with CS and CS-MNPs, a significant AF increase of O_{1s} at 533 eV was found. The reason might be that –OH of CS might have an interaction with the Fe atoms of MNPs, which induced the formation of –OH–Fe. Then the AF at 531.5 eV decreased (from 70.2 to 21.7%) and the AF around 533.0 eV increased (form 29.8 to 61.3%).

3.4. Hydrodynamic Size of CS-MNPs

The hydrodynamic (HD) size of CS-MNPs has a significant effect on its fate *in vitro* (e.g., residence time in bloodstream, probability of endocytosis, location in organ) [4]. The HD size of CS-MNPs was determined by laser light scattering at pH 5.0 (Fig. 6) to be 21.1 nm with a polydispersity index of 0.29, which makes it feasible to pass the vascular organization and result in internalization of the CS-MNPs. As the HD size of the CS-MNPs includes the coating layer (CS in this case), that shows swelling behavior in aqueous solution, the HD size is larger than the size determined by TEM (10 nm). Moreover, a slight aggregation of CS-MNPs may also increase the HD size.

3.5. In Vitro *Cell Viability and Cytotoxicity Study*

To evaluate the cytotoxicity of CS-MNPs, different concentrations of CS-MNPs were used (0.05, 0.1, 0.2 mg/ml). The amount of viable cells was obtained by the MTT cell proliferation assay and the results are shown in Fig. 7. Cells cultured with medium only were used as control. After 24 and 48 h incubation only a slight decrease in cell viability was observed for all tested concentrations. After 24 h incubation, the cell viability was 96, 92 and 87%, respectively. Over 83% cell viability

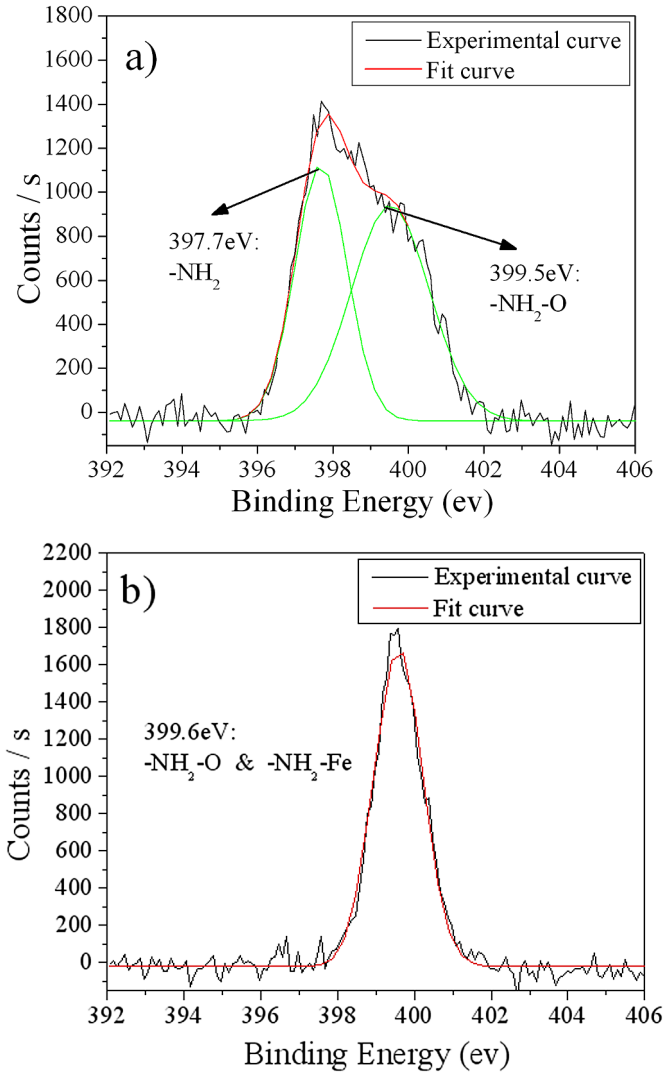

Figure 4. The N_{1s} XPS spectra of (a) chitosan and (b) CS-MNPs. This figure is published in colour in the online edition of this journal, which can be accessed *via* http://www.brill.nl/jbs

was still observed after 48 h of incubation at concentrations of up to 0.2 mg/ml. In conclusion, the MTT assay shows that the CS-MNPs do not express an acute adverse effect on MG-63 cells at doses up to 0.2 mg/ml, suggesting that the CS-MNPs are suitable as drug carrier for *in vivo* applications.

3.6. Cellular Uptake of CS-MNPs

In order to identify the location of the CS-MNPs in the MG-63 cells, TEM morphologies of MG-63 cells after 48 h incubation were determined (Fig. 8). With CS-

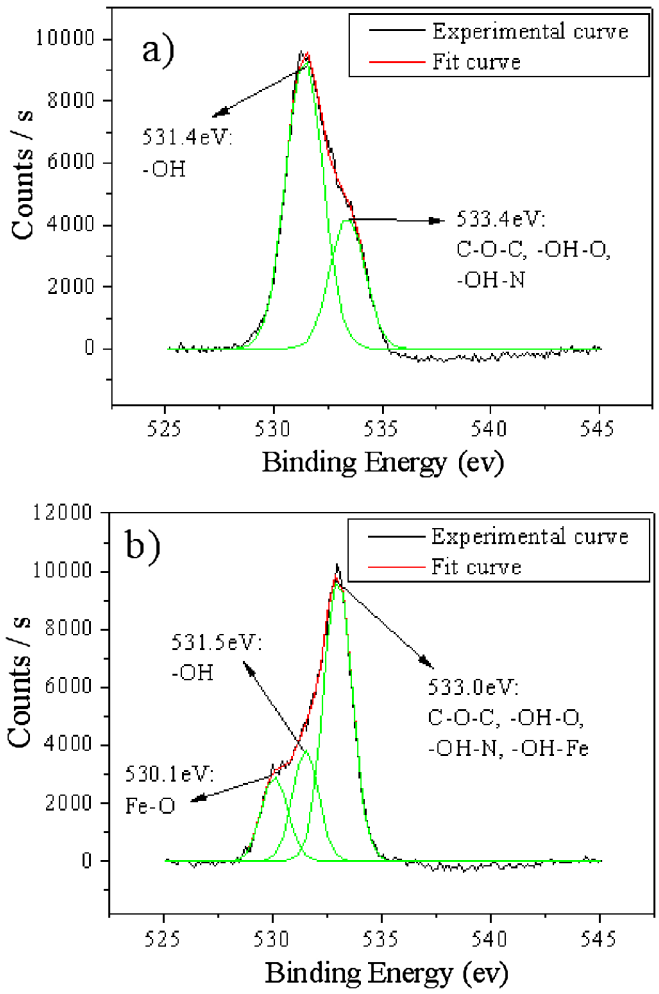

Figure 5. The O_{1s} XPS spectra of (a) chitosan and (b) CS-MNPs. This figure is published in colour in the online edition of this journal, which can be accessed *via* http://www.brill.nl/jbs

MNPs concentration increasing from 0.05 to 0.2 mg/ml, the intracellular iron concentrations of MG-63 cells increased from 29.4 ± 3.6 to 78.4 ± 8.5 pg/cell for 48 h incubation (for details, see the Appendix). The CS-MNPs (red virtual circled area) was present in the form of agglomerates in MG-63 cells and distributed rather randomly in the cytoplasm (such as cytosol, lysosome and vacuole). No CS-MNPs was detected in the mitochondria and nucleus (for details, see the Appendix). Several cellular uptake mechanisms have been identified: clathrin-mediated endocytosis, caveolae, macropinocytosis and phagocytosis. Caveolae (approx. 50 nm in diameter) and phagocytosis (only occurring in specialized cells, such as macrophages) are not involved for intracellular uptake of CS-MNPs. The nanoparticles internalized *via* clathrin-mediated endocytosis are generally entrapped in the intracellular

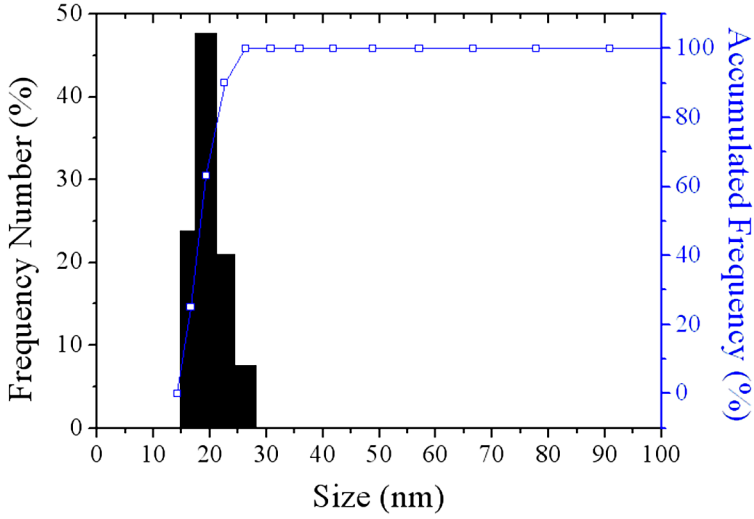

Figure 6. The HD size of CS-MNPs determined by laser light scattering. This figure is published in colour in the online edition of this journal, which can be accessed *via* http://www.brill.nl/jbs

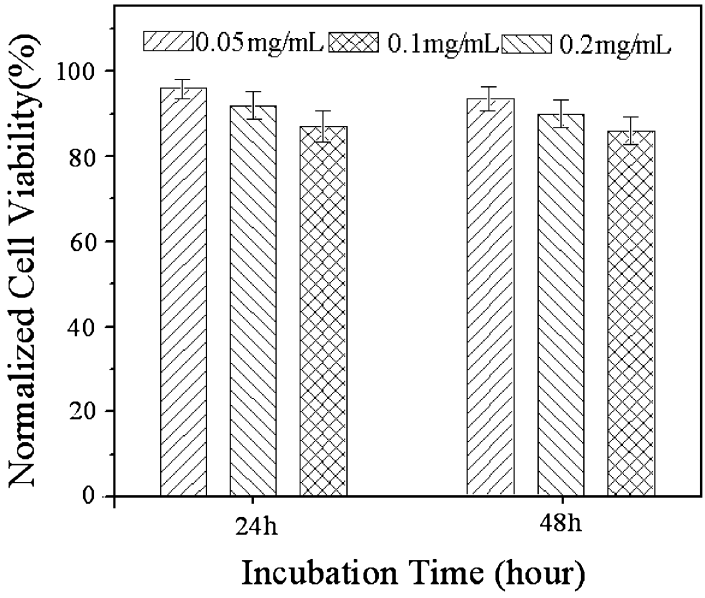

Figure 7. Cytotoxicity of CS-MNPs with different concentrations (0.05, 0.1 and 0.2 mg/ml) and different times (24 and 48 h). The cell viability was normalized to the control cells which were cultured with cell medium only.

vesicles (approx. 100 nm in diameter). However, the CS-MNPs were distributed randomly in MG-63 cells, which validated that the main endocytosis mechanism is macropinocytosis (0.5–5 μm in diameter) rather than clathrin-mediated endocyto-

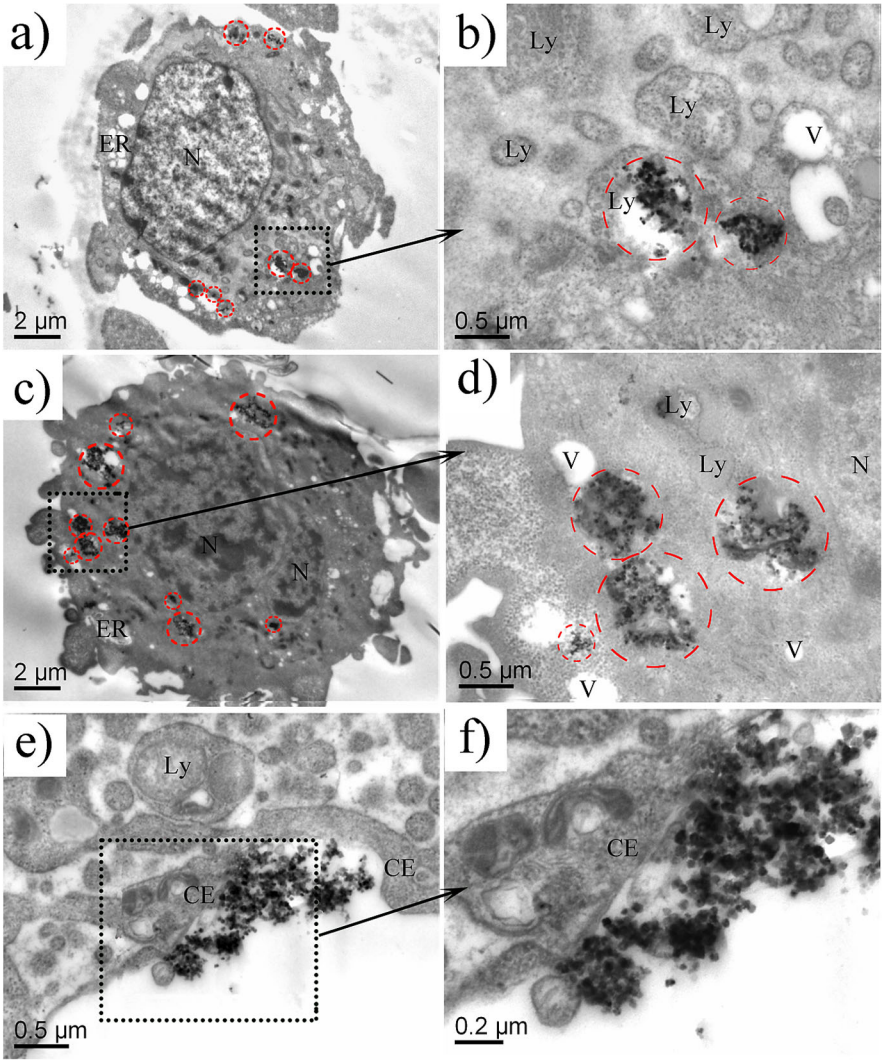

Figure 8. Morphologies and location of CS-MNPs in MG-63 cells. (a and b) The dose of CS-MNPs was 0.05 mg/ml; (c and d) the dose of CS-MNPs was 0.2 mg/ml; (e and f) CS-MNPs enter the MG-63 cell *via* macropinocytosis. N, nucleus; Ly, lysosome; Mt, mitochondria; ER, endoplasmic reticulum; V, vacuole; CM, cell membrane. This figure is published in colour in the online edition of this journal, which can be accessed *via* http://www.brill.nl/jbs

sis. The images of CS-MNPs entering the MG-63 cell are shown in Fig. 8e and f, which also indicated that MG-63 cells can internalize CS-MNPs *via* macropinocytosis. Macropinocytosis, compared with the clathrin-mediated endocytosis pathway which results in the degradation of internalized nanoparticles by lysosome [26], is a promising alternative to the clathrin-mediated endocytosis, avoiding degradation of the CS-MNPs by lysosomes.

4. Conclusions

CS-MNPs, which have magnetite as nano-core and CS as coating layer, were synthesized *via* a facile single-step method. Compared with the ligands with an O atom, CS with plenty of amino groups as coating layer induced CS-MNPs with high saturated magnetization (55.5 emu/g). The 24% CS layer of CS-MNPs makes it highly biocompatible. MTT assay shows that the CS-MNPs do not express acute adverse effect on MG-63 cells at doses up to 0.2 mg/ml. Macropinocytosis is the main endocytic mechanism of MG-63 cells to internalize CS-MNPs, which might avoid lysosomal degradation of the CS-MNPs. These special properties of CS-MNPs make it have potential applications in the field of targeted drug delivery, separation for purification and immunoassay and magnetic resonance imaging (MRI).

Acknowledgements

The authors thank the financial support from National Science Foundation of China (50702017), Innovation Foundation of HIT (HIT.NSRIF.2008.51) and State Key Laboratory of Urban Water Resource and Environment of HIT (2010QN05).

References

1. A. Sasco, *J. Biomed. Pharmacother.* **62**, 110 (2008).
2. M. Parkin, F. Bray, J. Ferlay and P. Pisani, *Cancer J. Clin.* **55**, 74 (2005).
3. D. Castellano, R. Hitt, C. F. Hernan, A. Romero and R. P. Luis, *J. Clin. Oncol.* **18**, 695 (2000).
4. M. Arruebo, F. P. Rodrigo, M. R. Ibarra and J. Santamaria, *Nanotoday* **2**, 22 (2007).
5. P. V. Kulkarni, J. Keshavayya and V. H. Kulkarni, *Polym. Adv. Technol.* **18**, 814 (2007).
6. J. H. Jeong, B. Y. Byun and T. G. Park, *J. Biomater. Sci. Polymer Edn* **14**, 1 (2003).
7. F. Gao, Y. Cai, J. Zhou, X. Xie, W. Ouyang, Y. Zhang, X. Wang, X. Zhang, X. Wang, L. Zhao and J. Tang, *Nano Res.* **3**, 23 (2010).
8. W. J. Parak, D. Gerion, T. Pellegrino, D. Zanche, C. Micheel, S. C. Williams, R. Boudreau, M. A. L. Gros, C. A. Larabell and A. P. Alivisatos, *Nanotechnology* **14**, R15 (2003).
9. J. H. Maeng, D. H. Lee, D. H. Jung, Y. H. Bae, I. S. Park, S. Jeong, Y. S. Jeon, C. K. Shim, W. Kim, J. Kim, J. Lee, Y. M. Lee, J. H. Kim, W. H. Kim and S. S. Hong, *Biomaterials* **31**, 4995 (2010).
10. F. Dilnawaz, A. Singh, C. Mohanty and S. K. Sahoo, *Biomaterials* **31**, 3694 (2010).
11. J. Zhang and R. D. K. Misra, *Acta Biomater.* **3**, 838 (2007).
12. N. Cordente, M. Respaud, F. Senocq, M. J. Casanove, C. Amiens and B. Chaudret, *Nano Lett.* **1**, 565 (2001).
13. F. Dang, N. Enomoto, J. Hojo and K. Enpuku, *Ultrason. Sonochem.* **17**, 193 (2010).
14. A. H. Lu, E. L. Salabas and F. Schuth, *Angew. Chem. Int. Edn* **46**, 1222 (2007).
15. L. F. Cotica, I. A. Santos, E. M. Girotto, E. V. Ferri and A. A. Coelho, *J. Appl. Phys.* **108**, 064325 (2010).
16. J. Sun, S. Zhou, P. Hou, Y. Yang, J. Weng, X. H. Li and M. Y. Li, *Biomed. Mater. Res.* **80A**, 333 (2007).
17. J. Hormes, H. Modrow, H. Bonnemann and C. S. S. R. Kumar, *J. Appl. Phys.* **97**, 10R102-1 (2005).

18. J. W. Lee, M. C. Jung, H. D. Park, K. D. Park and G. H. Ryu, *J. Biomater. Sci. Polymer Edn* **15**, 1065 (2004).
19. H. S. Lee, H. P. Shao, Y. Q. Huang and B. K. Kwak, *IEEE T. Magn.* **41**, 4102 (2005).
20. H. Honda, A. Kawabe, M. Shinkai and T. Kobayashi, *J. Ferment. Bioeng.* **86**, 192 (1998).
21. Y. Q. Ge, Y. Zhang, S. Y. He, F. Nie, G. J. Teng and N. Gu, *Nanoscale. Res. Lett.* **4**, 287 (2009).
22. G. Y. Li, Y. R. Jiang, K. L. Huang, P. Ding and L. L. Yao, *Colloids Surfaces A* **320**, 11 (2008).
23. M. A. Willard, L. K. Kurihara, E. E. Carpenter, S. Calvin and V. G. Harris, *Int. Mater. Rev.* **49**, 125 (2004).
24. F. Y. Cheng, C. H. Su, Y. S. Yang, C. S. Yeh, C. Y. Tsai, C. L. Wu, M. T. Wu and D. B. Shieh, *Biomaterials* **26**, 729 (2005).
25. M. Mikhaylova, Y. S. Jo, D. K. Kim, N. Bobrysheva, Y. Andersson, T. Eriksson, M. Osmolowsky, V. Semenov and M. Muhammed, *Hyperfine Interact.* **156–157**, 257 (2004).
26. S. D. Conner and S. L. Schmid, *Nature* **422**, 37 (2003).
27. M. Das, D. Mishra, T. K. Maiti, A. Basak and P. Pramanik, *Nanotechnology* **19**, 415101 (2008).
28. Y. Zhang, N. Kohler and M. Q. Zhang, *Mater. Res. Soc. Symp. Proc.* **676**, Y9.8.1 (2001).
29. M. M. Lin, S. Li, H. H. Kim, H. Kim, H. B. Lee, M. Muhammed and D. K. Kim, *J. Mater. Chem.* **20**, 444 (2010).

Appendix

A.1. Intracellular Iron Concentration

The intracellular iron concentration was obtained from the equation below as follows:

$$C_{\mathrm{Fe}} = \frac{S_{\mathrm{Fe_3O_4}}}{S_{\mathrm{cell}}} \cdot V_{\mathrm{cell}} \cdot \rho_{\mathrm{Fe_3O_4}} \cdot \frac{3M_{\mathrm{Fe}}}{M_{\mathrm{Fe_3O_4}}},$$

where $S_{\mathrm{Fe_3O_4}}$ is the area of MNPs from TEM morphology, S_{cell} is the area of MG-63 cell from TEM morphology, V_{cell} is the volume of MG-63 cell, $\rho_{\mathrm{Fe_3O_4}}$ is the density of magnetite (5.18 g/cm^3), M_{Fe} is the molecular weight of iron and $M_{\mathrm{Fe_3O_4}}$ is the molecular weight of magnetite. Image-Pro-Plus 5.0 was used to analyze the TEM micrographs for $S_{\mathrm{Fe_3O_4}}$ and S_{cell}. At least six TEM micrographs were used for each concentration. With the increase of CS-MNPs concentration from 0.05 mg/ml to 0.2 mg/ml, the intracellular iron concentrations of MG-63 cells expressed an increase from 29.4 ± 3.6 pg/cell to 78.4 ± 8.5 pg/cell for 48 h incubation. Student's t-test was performed and it was found that the results obtained at concentrations of 0.05 and 0.2 mg/ml were statistically significant ($P < 0.007$). It has been reported that MG-63 cell-uptake levels of folate-magnetite and PEG-magnetite were low and similar to non-targeted controls [27]. After incubation at 0.2 mg/ml for 48 h, the intracellular iron concentrations for naked-magnetite, folate-magnetite and PEG-magnetite were 18, 15 and 20 pg/cell, respectively [28]. However, for the same dosage and same incubation time, the MG-63 cell-uptake level of CS-MNPs was higher (78.4 pg/cell), proving that the CS layer of CS-MNPs improve the cell internalization and ability to target MG-63 cells.

A.2. Crystal Structure of the Synthesized CS-MNPs

The CS-MNPs prepared through the one-step method were characterized by XRD and the result is shown in Fig. A1. The XRD pattern of CS-MNPs matches the pattern for magnetite (19-0629). Peaks for magnetite, marked by their indices ((111), (220), (311), (400), (422), (511), (440), (533)), were observed. The broad peak around 20° was assigned to chitosan layer of CS-MNPs. Because of the similar patterns between Fe_3O_4 and γ-Fe_2O_3, Raman spectroscopy was used to characterize the CS-MNPs (Fig. A2). The synthesized CS-MNPs showed a peak at 667 cm^{-1},

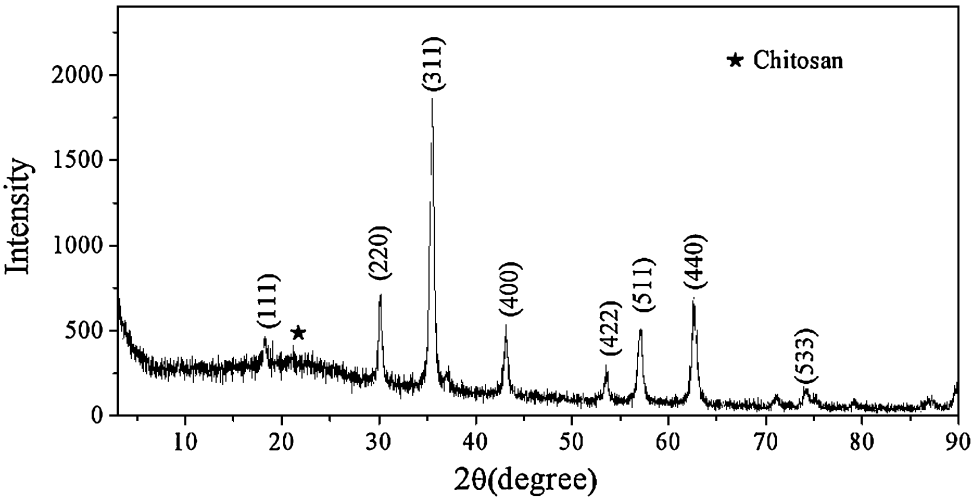

Figure A1. The XRD pattern of synthesized CS-MNPs.

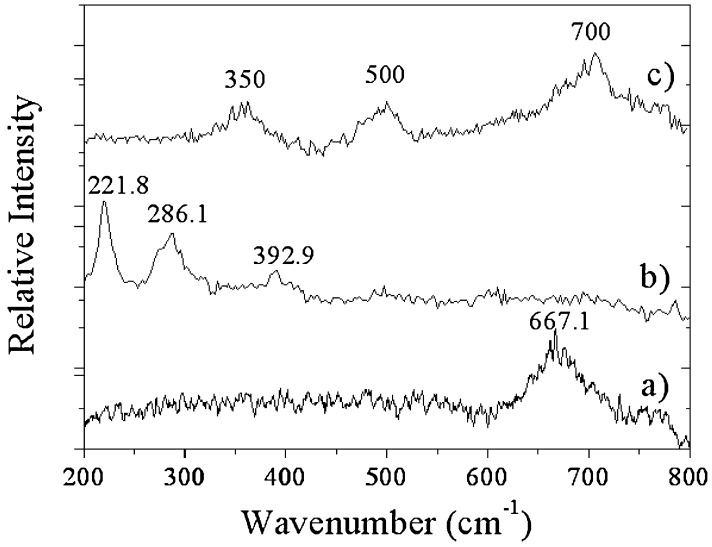

Figure A2. The Raman spectra of CS-MNPs (a), α-Fe_2O_3 (b) and γ-Fe_2O_3 (c).

which indicated that the magnetic nanoparticles were magnetite, rather than α-Fe_2O_3 or γ-Fe_2O_3.

A.3. FT-IR Spectrum and Surface Charge of CS-MNPs

In order to identify the surface state of CS-MNPs, the FT-IR spectrum of CS-MNPs was recorded (Fig. A3). Also, the spectrum of naked magnetite was given for comparison. As can be seen in Table A1, the absorption bands at 559 and 580 cm^{-1} corresponded to the Fe–O of magnetite. The bands at 2922, 2876 and 1372 cm^{-1}

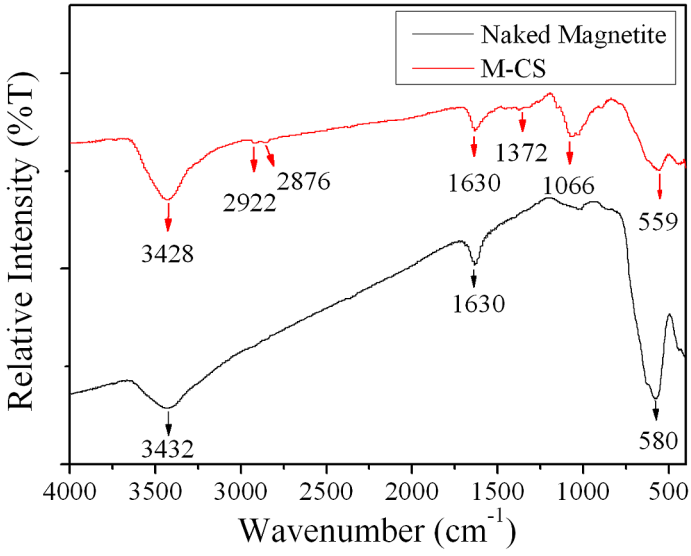

Figure A3. The FT-IR spectra of CS-MNPs (red curve) and naked magnetite (black curve). This figure is published in colour in the online edition of this journal, which can be accessed *via* http://www.brill.nl/jbs

Table A1.
Assignments of absorption bands of naked magnetite and CS-MNPs

	Absorption band (cm^{-1})	Assignment
Naked magnetite	580	Fe–O
	1630	–OH
	3432	–OH
CS-MNPs	559	Fe–O
	1066	νC–O
	1372	νCH
	1630	–OH and $–NH_2$
	2876	νCH
	2922	νCH
	3428	–OH and $–NH_2$

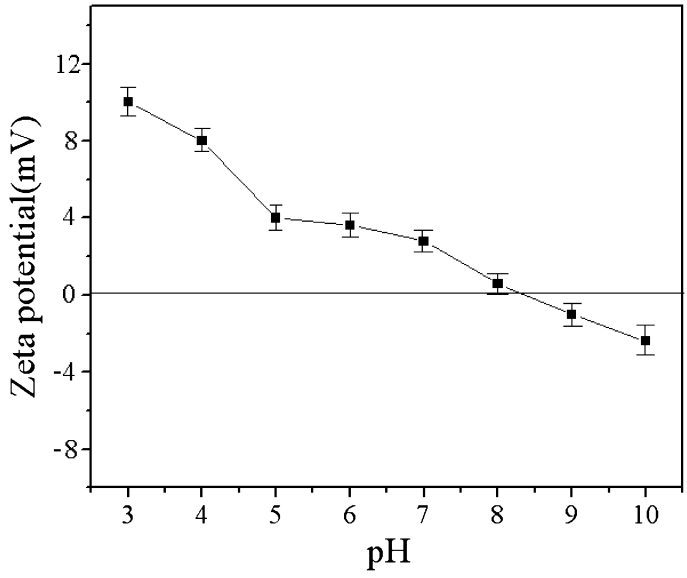

Figure A4. Zeta potential of the CS-MNPs as a function of pH.

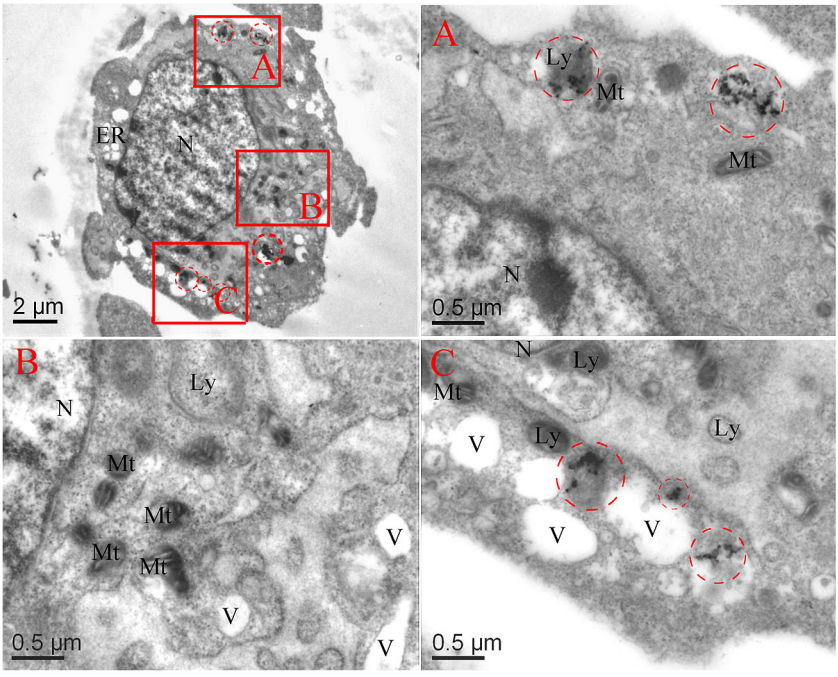

Figure A5. Detailed morphology of CS-MNPs in MG-63 cell (CS-MNPs dose 0.05 mg/ml). (A) Some of the CS-MNPs were localized in the lysosome and cytosol. (B) No CS-MNPs were detected in the endoplasmic. (C) CS-MNPs were localized in the endoplasmic reticulum. N, nucleus; Ly, lysosome; Mt, mitochondria; ER, endoplasmic reticulum; V, vacuole; CM, cell membrane. This figure is published in colour in the online edition of this journal, which can be accessed *via* http://www.brill.nl/jbs

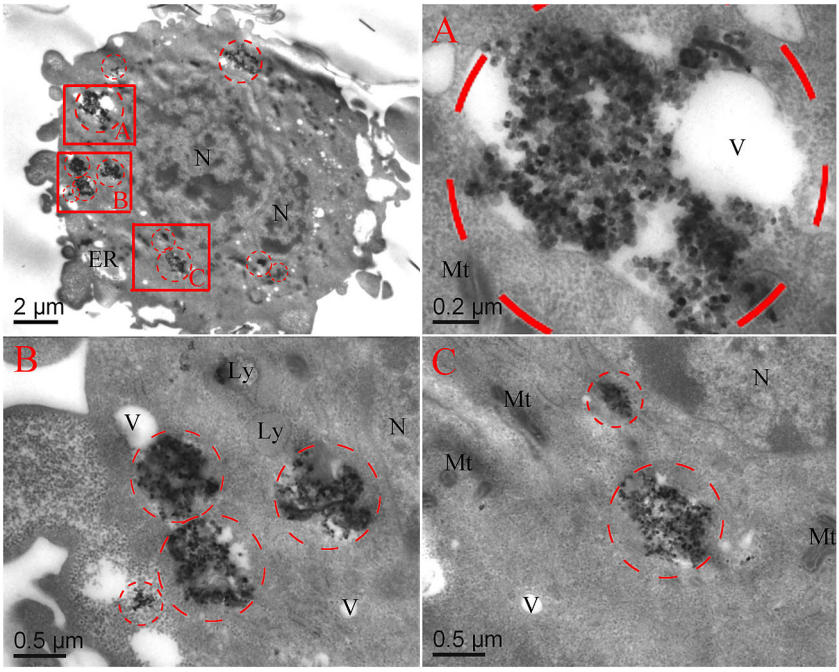

Figure A6. Detailed morphology of CS-MNPs in MG-63 cell (CS-MNPs dose 0.2 mg/ml). (A) Some of the CS-MNPs were localized in the vacuole. (B and C) Some of the CS-MNPs were localized in the cytosol. N, nucleus; Ly, lysosome; Mt, mitochondria; ER, endoplasmic reticulum; V, vacuole; CM, cell membrane. This figure is published in colour in the online edition of this journal, which can be accessed *via* http://www.brill.nl/jbs

of CS-MNPs were attributed to νCH of chitosan. Moreover, the absorption band at 1066 cm^{-1} (which was attributed to νC–O of chitosan) proved the existence of the chitosan layer in CS-MNPs.

The surface charges of the nanoparticles influence the metabolism of the CS-MNPs *in vivo*. Zeta potential can give the surface states of the CS-MNPs. Figure A4 shows the zeta potential of the synthesized CS-MNPs as a function of pH. CS-MNPs were positively charged at low pH (<8.0) and negatively charged at high pH (>8.0). The CS-MNPs shows an isoelectric point (pI) of 8.0. An exciting phenomenon of CS-MNPs is that CS-MNPs show positive charge at physiological pH (7.4) due to the protonation of amino groups from the CS layer. Compared with carboxyl modified magnetite whose pI was 4.3 [29], the cationic CS-MNPs can easily adhere to the cell membrane (containing negatively charged phospholipids), which make it convenient for CS-MNPs to enter the targeted cells.

A.4. Cellular Uptake of CS-MNPs

MG-63 cell line, a human osteosarcoma cell line was used in the *in vitro* tests. In order to identify the location of the CS-MNPs in the MG-63 cells, TEM morphologies were given (Figs A5 and A6). With the increase of CS-MNP concentration during

incubation, the amount of CS-MNPs into the cells increased. From the magnified images, it can be seen that the CS-MNPs (red virtual circled area) was present in the form of agglomerates in MG-63 cells and most of the agglomerates were distributed rather randomly in cytoplasm of MG-63. No CS-MNPs was detected in mitochondria and in the nucleus.